IET Power Electronics

Special Issue: Advanced Technologies Utilised in Wireless Power Transfer Systems

IET Journals
The Institution of Engineering and Technology

Interoperability study of fast wireless charging and normal wireless charging of electric vehicles with a shared receiver

ISSN 1755-4535
Received on 11th October 2018
Revised 14th January 2019
Accepted on 25th February 2019
E-First on 18th March 2019
doi: 10.1049/iet-pel.2018.6080
www.ietdl.org

Yiming Zhang[1], Zhengchao Yan[1,2], Tianze Kan[1], Chris Mi[1] ✉

[1]*Department of Electrical and Computer Engineering, San Diego State University, 5500 Campanile Drive E426A, San Diego, USA*
[2]*School of Marine Science and Technology, Northwestern Polytechnical University, 127 West Youyi Road, Xi'an, People's Republic of China*
✉ *E-mail: mi@ieee.org*

Abstract: Fast charging of electric vehicles (EVs) has been the trend recently. For conductive charging, normal charging can be realised by an on-board charger, while fast charging can be realised by a DC charger which is usually off-board the vehicle. However, for wireless charging, there is a need of a transmitter on the ground and a receiver on the EV side. Therefore, there will be a high-power receiver and a low-power receiver in one EV to achieve dual charging capabilities. To reduce the EV-side cost, weight, and volume, this paper proposes a wireless charging system with a shared receiver compatible of fast wireless charging (FWC) at a small air gap and normal wireless charging (NWC) at a large air gap. The relationship between the coil size and the power level is investigated and a suitable receiver coil size is selected for FWC. The LCC-LCC topology is selected due to its characteristic of output power proportional to the coupling coefficient. Design procedures of the receiver and transmitters are investigated. The simulations and the experimental results obtained from the downscaled prototype verified the effectiveness of the compatibility design.

1 Introduction

Wireless power transfer (WPT) [1–4] is an emerging technology that has achieved a great advancement in academia and a deep penetration into the commercial market. Electric vehicle (EV) wireless charging is a typical application of the WPT technology [5, 6]. Compared with conductive charging, wireless charging has the advantages of convenience (free from manual operation) [7], safety (free from electric shock and sparks), reliability (free from water and dust), and applicability in harsh environments [8, 9]. However, cost, size, charging time, and efficiency are the barriers that affect the application of EV wireless charging.

The charging time is one of the major concerns of EV charging. Take Tesla Model S as an example. The battery capacity in the standard edition is 75 kWh. To fully charge Tesla Model S from 15% state of charge, it takes over 9 h for a 7 kW charger; while only 32 min are spent for a fast charger rated at 120 kW. Thus, fast charging is one of the future trends that shorten the charging time for EVs. Tesla has developed a supercharger capable of 120 kW conductive charging [10]. For wireless charging, there is a need of a transmitter on the ground and a receiver on the EV side. Fast wireless charging (FWC) is needed for an EV to shorten the charging time, which normally occurs in the charging station, where high-power charging facilities are available. Normal wireless charging (NWC) is also required for an EV, which mainly takes places in the residential or public garages, where only low-power charging facilities are available. Therefore, to enable the EV for FWC and NWC, there will be two sets of receivers, resulting in high cost, bulky size, and heavy weight on the EV side. To address these issues, power interoperability of NWC and FWC should be studied.

Table 1 Design requirements for two charging scenarios

Parameter	FWC	NWC (J2954)
charging location	Charging Station	Residential Garage
output power	120 kW	7 kW
charging distance	35 mm	150 mm
misalignment issue	No	Max (75 mm, 100 mm)
operating frequency	<85 kHz	85 kHz
inverter DC voltage	<800 V	<650 V
rated battery voltage	320 V	320 V

For purposes of compatibility, the receiver in a WPT system should be interoperable with different transmitters, and vice versa. Current literature in this area focuses on (i) battery voltage compatibility [11], where battery packs with the voltage ranging from 250 to 700 V could be wirelessly charged by inserting either a buck or a boost converter; (ii) coil compatibility [12–14], where different coil shapes, such as circular coil, bipolar coil, and DD coil, were compared and tested; (iii) power compatibility, where the transmitter was designed for receivers with different power levels [15, 16]; (iv) frequency compatibility, where dual-frequency operation was studied for low-power applications [17, 18]. However, there is a lack in designing a receiver capable of both FWC and NWC.

To achieve dual power capability of FWC and NWC using a shared receiver with reduced EV-side cost, weight, and volume, the shared receiver and the respective transmitters should be carefully designed. FWC and NWC have different charging scenarios. Usually the charging distance of FWC shall be designed to be very small so that the power density can be improved and the coil size and system cost can be reduced. A mechanical positioning device can be employed to accurately adjust the charging position. Thus, there are no misalignment issues for FWC. In comparison, the charging distance of NWC is usually large, approximately 100–200 mm. If no mechanical device is utilised, there will be a misalignment issue. The maximum misalignment is set to 75 mm in the front-to-rear direction and 100 mm in the door-to-door direction according to the recommended practice J2954 from the Society of Automotive Engineers. The typical design requirements for the two charging scenarios are summarised in Table 1.

This paper proposes a wireless EV charging system capable of FWC and NWC with a shared receiver. The design procedures of both FWC and NWC following Table 1 are performed and a downscaled system is implemented to validate the analysis.

2 Coil size and power level

To design a receiver compatible of 120 and 7 kW transmitters, the receiver coil size should be first determined. This section

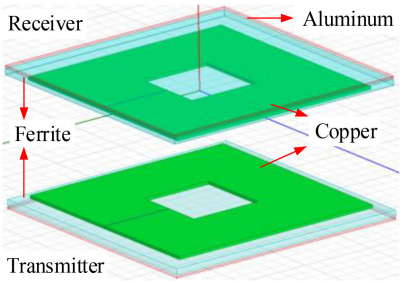

Fig. 1 *Model of a single-turn coil*

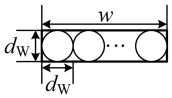

Fig. 2 *Cross section of a tightly wound coil*

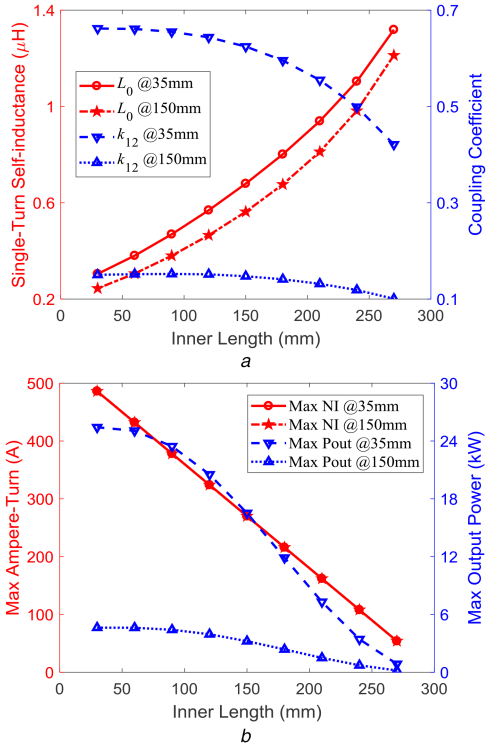

Fig. 3 *Simulation results*
(a) L_0 and k_{12} vs. IL,
(b) NI and P_{out} vs. IL

investigates the relationship between the coil size and the power level.

2.1 Maximum output power

For an inductive WPT system, the active transferred power of two coupled coils is maximised when the phase difference between the coil currents is 90° [19]. Under this condition, the output power can be expressed by

$$P_{trn} = \omega k_{12}\sqrt{L_1 L_2} I_1 I_2 = k_{12}\omega\sqrt{L_{10}L_{20}}(n_1 I_1)(n_2 I_2)\,. \tag{1}$$

where ω is the operating angular frequency, I_1 (I_2), L_1 (L_2), L_{10} (L_{20}), n_1 (n_2), and $n_1 I_1$ ($n_2 I_2$) are the current root-mean-square (RMS) value, the self-inductance, the single-turn self-inductance, the turn number, and the ampere-turn of the transmitter (receiver). k_{12} is the coupling coefficient. The single-turn inductance has the same coil dimension as the original coil, such as outer length (OL) and inner length (IL), but with only one turn, as shown in Fig. 1. Once the single-turn inductances L_{10} and L_{20} are obtained from the simulation, the actual inductances can be calculated by $L_1 = L_{10} \times n_1^2$ and $L_2 = L_{20} \times n_2^2$.

When the coil dimensions are determined, the maximum output power can be determined by the ampere-turn of the coils, which is maximised when the coil is tightly wound and can be calculated by its dimension and the withstanding current density. The cross-section of a tightly wound coil is shown in Fig. 2, where the coil layer is 1, the coil width is w, and the diameter of the litz wire is d_W. The area of the cross-section can be expressed by $S = w \times d_W$. Assume the litz wire has N_{ST} strands with a strand radius of r_S, and the utilisation ratio of the copper in the cross-section u_r can be calculated as

$$u_r = k_{UR} N_{ST} \frac{\pi r_S^2}{d_W^2}, \tag{2}$$

where k_{UR} is the coefficient that takes into consideration the fact that the wires cannot be tightly wound in reality. When the current density flowing through the copper is J, the maximum ampere-turn of a coil can be expressed as

$$(nI)_{max} = S u_r J\,. \tag{3}$$

For coils with ferrites, k_{12}, L_{10}, and L_{20} in (1) can be obtained through finite element simulation. Hence, the theoretical maximum power level of coupled identical coils can be obtained by

$$P_{trn-max} = k_{12}\omega\sqrt{L_{10}L_{20}}(S u_r J)^2\,. \tag{4}$$

2.2 Impact of IL

In J2954, the receiving coil size for the standard 7.7 kW charging was recommended to be 300 mm. Therefore, in this study, we start with the size of 300 mm × 300 mm × 4 mm to study the impact of the coil size. Two charging distances are selected: 35 and 150 mm.

The simulated single-turn self-inductance (L_0) and k_{12} varying with IL are plotted in Fig. 3*a*. L_0 increases with the increasing IL, and this can be explained by the fact that the coil mean length increases with the increasing IL. k_{12} decreases with the increasing IL, and when IL is smaller than one-third of OL, k_{12} will saturate.

To calculate the maximum output power, the operating frequency is set to 85 kHz as recommended by J2954 and J is assumed to be 3 A/mm^2. An 800-strand litz wire with a strand radius of 0.05 mm is suitable for this frequency. u_r is calculated to be 0.3. The calculated maximum ampere-turn and output power are shown in Fig. 3*b*. Both the ampere-turn and the output power decrease with the increasing IL. The maximum ampere-turn has nothing to do with the coupling coefficient and it is only determined by the coil geometry and current density, as shown in (3). Given the coupling coefficient and the maximum output power, IL is selected to be one-third of OL.

2.3 Impact of OL

Under the aforementioned conditions and IL is set to one-third of OL, the simulated L_0, k_{12}, nI, and P_{out} varying with OL are depicted in Fig. 4. Only when OL exceeds 450 mm, 120 kW output can be achieved.

The selection of J affects the maximum power level. When $J >$ 3 A/mm^2, a higher maximum output power can be achieved, but the cooling of the litz wires should be taken into consideration. Another factor that impacts the selection of the ampere-turn is the saturation of ferrite, which can be avoided by increasing the ferrite thickness.

3 Full-Scaled system design

3.1 Topology selection

The series-series (SS) and LCC-LCC topologies are two popular topologies in a WPT system due to the constant-current output

characteristic. They are compared to find a better solution to satisfy the design requirements. The equivalent circuits of the SS and LCC-LCC topologies are shown in Fig. 5, where U_1 (U_2) is the inverter (rectifier) AC voltage, L_1 (L_2), L_{f1} (L_{f2}), C_1 (C_2), and C_{f1} (C_{f2}) are main coil inductance, the auxiliary coil inductance, the series compensation capacitance, and the parallel compensation capacitance of the transmitter (receiver), respectively.

For the SS topology, the resonant frequency is

$$\omega = \frac{1}{\sqrt{L_1 C_1}} = \frac{1}{\sqrt{L_2 C_2}}. \tag{5}$$

In this condition, the output power of the SS topology can be expressed by

$$P_{out} = \frac{U_1 U_2}{\omega M_{12}} = \frac{1}{k_{12}} \frac{U_1 U_2}{\omega \sqrt{L_1 L_2}}. \tag{6}$$

For the LCC-LCC topology, the resonant frequency is

$$\begin{aligned} \omega &= \frac{1}{\sqrt{L_{f1} C_{f1}}} = \frac{1}{\sqrt{L_{f2} C_{f2}}} \\ &= \frac{1}{\sqrt{L_1 \dfrac{C_1 C_{f1}}{C_1 + C_{f1}}}} = \frac{1}{\sqrt{L_2 \dfrac{C_2 C_{f2}}{C_2 + C_{f2}}}}. \end{aligned} \tag{7}$$

In this condition, the output power of the LCC-LCC topology can be expressed by

$$P_{out} = \frac{\omega M_{12} U_1 U_2}{\omega L_{f1} \omega L_{f2}} = \frac{k_{12}}{\alpha_1 \alpha_2} \frac{U_1 U_2}{\omega \sqrt{L_1 L_2}} \tag{8}$$

where α_1 and α_2 are defined as

$$\alpha_1 = \frac{L_{f1}}{L_1}, \quad \alpha_2 = \frac{L_{f2}}{L_2}. \tag{9}$$

Comparing (6) with (8), we can see that the output power of the SS topology increases with the decreasing k_{12}, while that of the LCC-LCC topology increases with the increasing k_{12}. In the application scenario, k_{12} of FWC is much larger than that of NWC. The characteristic of the LCC-LCC topology facilitates the design of a receiver compatible of two distinctly different power levels. Moreover, there are two extra degrees of freedom, namely α_1 and α_2, to help the design of such a WPT system. Therefore, the LCC-LCC topology is selected.

3.2 Coil design

In the two charging scenarios, there is only one receiver, but the receiver is at two different charging distances. Thus, the self- and mutual inductances vary but the capacitances keep the same. Therefore, there are two sets of parameters for one receiver. The equivalent circuits of the two charging scenarios are shown in Fig. 6, where L_{21} (L_{22}) and L_{f21} (L_{f22}) are the receiver main coil and auxiliary coil inductances of FWC (NWC). M_{121} and M_{322} are the mutual inductances. The single-turn inductances are denoted by adding 0 in the subscript (L_{210}, L_{220}, L_{f210}, and L_{f220}).

One of the problems with the shared receiver using the LCC-LCC topology is that L_{21} differs greatly from L_{22} at the two charging distances of 35 and 150 mm, but C_2 and C_{f2} remain the same. If L_{f21} and L_{f22} are the same, the receiver will not work in resonance for both scenarios. That means if the parameters are tuned for one charging scenario, the parameters for the other will be detuned due to the variation of the main coil inductance. The solution to this issue is to integrate the auxiliary coil with the main coil and carefully design the coils so that the receiver works in resonance for both case, i.e.

$$\begin{cases} f_{FWC} = \dfrac{1}{\sqrt{L_{f21} C_{f2}}} = \dfrac{1}{\sqrt{L_{21} \dfrac{C_2 C_{f2}}{C_2 + C_{f2}}}} \\ f_{NWC} = \dfrac{1}{\sqrt{L_{f22} C_{f2}}} = \dfrac{1}{\sqrt{L_{22} \dfrac{C_2 C_{f2}}{C_2 + C_{f2}}}} \end{cases} \tag{10}$$

which can be transformed into

$$\frac{L_{f210}}{L_{f220}} = \frac{L_{210}}{L_{220}}. \tag{11}$$

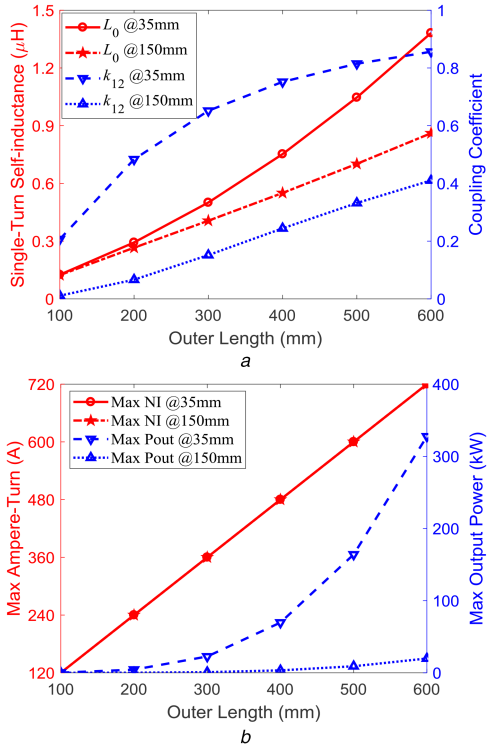

Fig. 4 *Simulation results*
(a) L_0 and k_{12} vs. OL,
(b) NI and P_{out} vs. OL

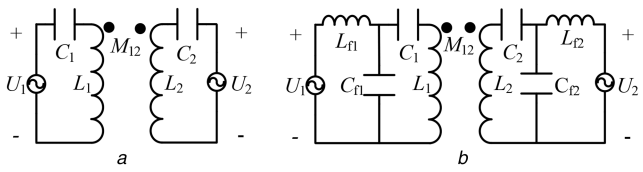

Fig. 5 *Equivalent circuits*
(a) SS,
(b) LCC-LCC

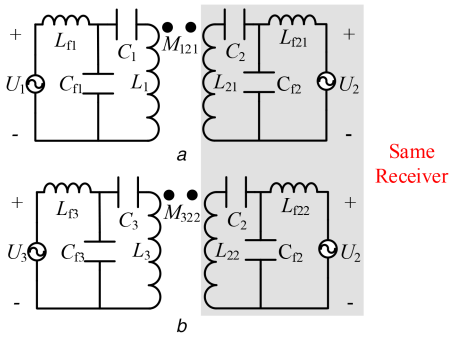

Fig. 6 *Equivalent circuits of LCC-LCC topology*
(a) FWC at 35 mm,
(b) NWC at 150 mm

We can see from (11) that the main coil inductance and the auxiliary coil inductance of the receiver should have the same variation rate. In this case, the relationship of the operating frequencies of the two charging scenarios can be expressed by

$$f_{\mathrm{FWC}} = \sqrt{\frac{L_{220}}{L_{210}}} f_{\mathrm{NWC}}. \tag{12}$$

For FWC, the coils are designed to be symmetrical. The main coils are unipolar coils and the auxiliary coils are bipolar coils which are perpendicular to each other, as depicted in Fig. 7. Thus, there is no coupling between L_{f1} and L_{f2}, or between L_{f1} and L_1, L_{f2} and L_2.

The size of the main coils is selected according to the maximum power level estimation of Section 2. The coil dimensions are given in Fig. 7. By changing the dimensions of the auxiliary coils of FWC, L_{f210} and L_{f220} can be adjusted to achieve (11). Since the receiver auxiliary coil is a bipolar coil, there are many parameters that can be changed to satisfy (11), such as the coil outer length, outer width, inner length, and inner width. One design instance is shown below. When the length of the bipolar coil is set to 500 mm and the coil width is 80 mm, the simulated single-turn self-inductances varying with the width of the bipolar coil are shown in Fig. 8. When the width of the bipolar coil is 500 mm, $L_{\mathrm{f210}} / L_{\mathrm{f220}} = L_{210} / L_{220}$. Therefore, the width of the bipolar coil is chosen to be 500 mm. The simulation results are listed in Table 2.

We can see from Table 2 that there is no major difference in the parameters between the perfect alignment and misalignment of NWC except for the coupling coefficient. The output power of the LCC–LCC topology increases with the increasing coupling coefficient. Therefore, for a given range of the inverter DC voltage, the parameters should be designed so that the output power of NWC at the maximum misalignment reaches the rated value, while for the perfect alignment case, the inverter DC voltage can be regulated for the rated output.

The output power of FWC and NWC with the maximum misalignment can be expressed, based on (8), as

$$P_{\mathrm{out-FWC}} = \frac{k_{121}}{\alpha_1 \alpha_2 n_1 n_2} \frac{U_1 U_2}{\omega_{\mathrm{FWC}} \sqrt{L_{10} L_{210}}} \tag{13}$$

$$P_{\mathrm{out-NWC}} = \frac{k_{322}}{\alpha_3 \alpha_2 n_3 n_2} \frac{U_3 U_2}{\omega_{\mathrm{NWC}} \sqrt{L_{30} L_{220}}} \tag{14}$$

where n_1, n_2, and n_3 are the turn numbers of L_1, L_{21} (L_{22}) and L_3, respectively.

When the operating frequency of NWC is 85 kHz, the operating frequency of FWC can be calculated, according to (12), as 68.1 kHz. For the two charging scenarios, α_2, n_2, and U_2 are the same, but k_{121}, k_{322}, L_{10}, L_{210}, L_{30}, and L_{220} are all determined by the coil geometry. Thus, only α_1, n_1, α_3, n_3, U_1 and U_3 can be adjusted for the two power levels. By substituting the parameters into (13) and (14), the relationship between the designed parameters of the transmitters can be expressed as

$$\frac{\alpha_3 n_3 U_1}{\alpha_1 n_1 U_3} = \frac{P_{\mathrm{out-FWC}}}{P_{\mathrm{out-NWC}}} \frac{k_{322}}{k_{121}} \sqrt{\frac{L_{10}}{L_{30}}} \simeq 4.14. \tag{15}$$

There are multiple combinations of the parameters α_1, n_1, α_3, n_3, U_1 and U_3 that can achieve the requirement of (15). One suitable solution is listed in Table 3.

The system design procedure is summarised in Fig. 9.

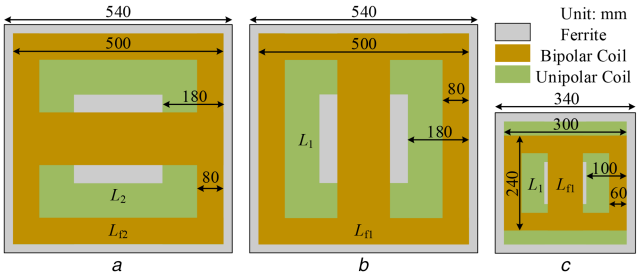

Fig. 7 *Coil geometry and dimension*
(a) Shared receiver,
(b) FWC transmitter,
(c) NWC transmitter

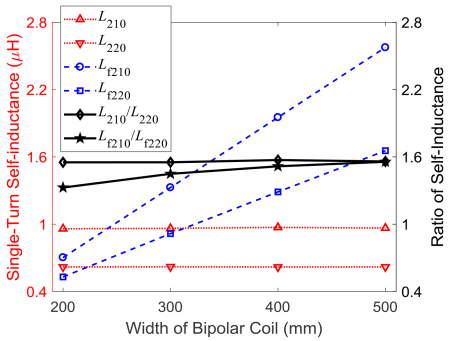

Fig. 8 *Simulated single-turn self-inductances and their ratios vs. width of bipolar coil*

Table 2 Simulated single-turn self-inductances and coupling coefficients

FWC (μH) (0 mm, 0 mm)		NWC (μH) (0 mm, 0 mm)		NWC (μH) (75 mm, 100 mm)	
L_{f10}	2.574	L_{f30}	0.518	L_{f30}	0.519
L_{10}	0.966	L_{30}	0.407	L_{30}	0.407
L_{f210}	2.575	L_{f220}	1.655	L_{f220}	1.627
L_{210}	0.965	L_{220}	0.619	L_{220}	0.628
k_{121}	0.810	k_{322}	0.192	k_{322}	0.127

Table 3 One suitable solution for power compatibility

Symbol	Value	Symbol	Value
n_{f1}	2	n_{f3}	7
n_1	6	n_3	11
n_{f2}	2	n_{f2}	2
n_2	6	n_2	6
L_{f1}	10.3 μH	L_{f3}	25.4 μH
L_1	34.7 μH	L_3	49.2 μH
L_{f21}	10.3 μH	L_{f22}	6.62 μH
L_{21}	34.7 μH	L_{22}	22.3 μH
C_{f1}	530.6 nF	C_{f3}	137.9 nF
C_1	223.6 nF	C_3	147.2 nF
C_{f2}	530.6 nF	C_{f2}	530.6 nF
C_2	223.6 nF	C_2	223.6 nF
f_{FWC}	68.1 kHz	f_{NWC}	85 kHz
U_{inv1}	750 V	U_{inv3}	440–630 V

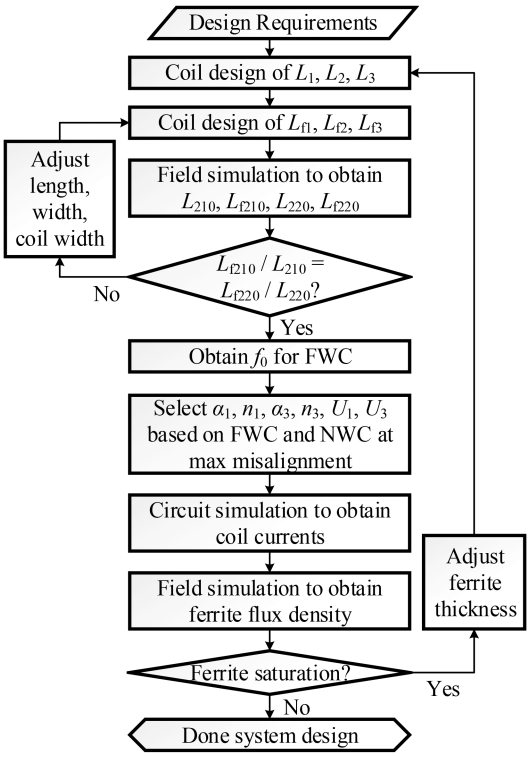

Fig. 9 *System design procedure*

3.3 Simulation

To validate the proposed solution in Table 3, the FWC and NWC systems are modelled in MATLAB/Simulink. The simulation results are listed in Table 4. The DC–DC efficiencies of these two charging systems are both over 94%. Thus, the design requirements have been satisfied to use the same receiver for two distinctively different power levels.

The simulation waveforms are shown in Fig. 10.

4 Downscaled system validation

Due to the power limitation in the lab, the 120 kW FWC system cannot be realised. Instead, a downscaled prototype of 6.4 and 1.0 kW is implemented. The charging distance of the 6.4 kW system is 15 mm and that of the 1.0 kW system is 142 mm so that approximately the same coupling coefficients as the full-scaled systems are achieved. Following the same procedures in Section II, the coils can be designed. The ferrite size is 448 mm × 354 mm × 8 mm, and the coil dimensions are labelled in Fig. 11. The photograph of the experimental setup is depicted in Fig. 12. The simulated and measured inductances are compared in Table 5. The largest misalignment is set to (75, 100 mm).

We can see from Table 5 that 85.9 / 59.0 ≈ 288.2 / 195.4. Therefore, the receiver can stay in resonance at both charging distances. The resonant frequency of the 1.0 kW system is set to be 85 kHz. Thus, the resonant frequency of the 6.4 kW is calculated to be $85 \times \sqrt{195.4/288} = 70$ kHz. $C_1 = C_2 = 24.85$ nF, $C_{f1} = C_{f2} = 59.16$ nF, $C_3 = 17.0$ nF, and $C_{f3} = 47.8$ nF. The rectifier DC voltage is set to 250 V, and the maximum inverter DC voltage is set to 450 V for the 6.4 kW system and the maximum inverter DC voltage is set to 300 V for the 1.0 kW system.

The RMS values of the coil currents are plotted in Fig. 13. The output power and the DC–DC efficiency of the two power levels are depicted in Fig. 14. The discrepancies of the output power for the 1.0 kW system is caused by the discontinuous rectifier current waveforms. Nevertheless, the DC–DC efficiencies of the two systems can be over 95%.

The experimental waveforms of the three cases are shown in Fig. 15.

Table 4 Simulation results of FWC and NWC

System, mm	FWC, 0, 0	NWC, 0, 0	NWC, 75, 100
U_{inv} (V)	750	440	630
P_{out} (kW)	120.2	6.97	6.99
η (%)	97.0	94.9	94.9
$I_{f1}(I_{f3})$ (A)	184.8	20.7	14.1
$I_1(I_3)$ (A)	152.8	28.9	40.1
I_{f2} (A)	417.1	28.7	29.0
I_2 (A)	66.9	80.6	77.8

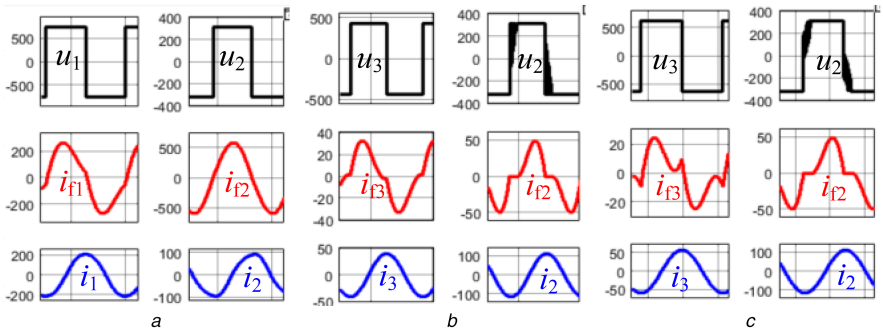

Fig. 10 *Simulation waveforms*
(a) FWC at (0 mm, 0 mm),
(b) NWC at (0 mm, 0 mm),
(c) NWC at (75 mm, 100 mm)

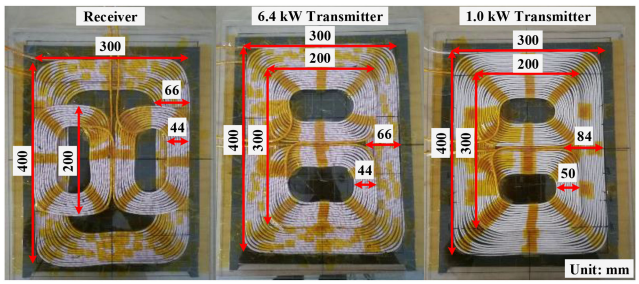

Fig. 11 *Coil dimensions of 6.4 and 1.0 kW systems*

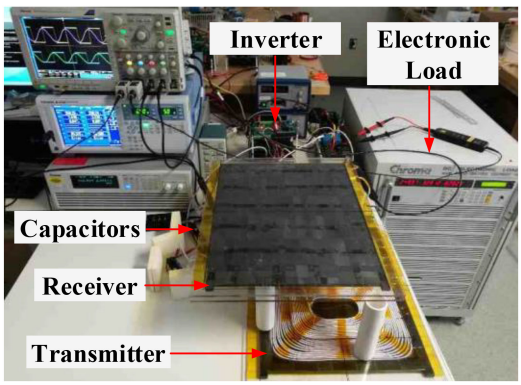

Fig. 12 *Photograph of experimental prototype for NWC at maximum misalignment*

5 Conclusion

This paper studied the compatibility of wireless charging of EVs at both high-power and normal power levels sharing the same receiver. Two different power levels, i.e. a 120 kW FWC at a 35 mm charging distance and a 7 kW NWC at a 150 mm charging distance, are achieved with relatively high efficiency using the LCC–LCC topology through simulation. The relationship between the coil size and the power level was investigated. For a given power level, the required coil size can be estimated. Based on the estimated coil size for the target power level, the wireless charging system compatible of FWC and NWC with the same receiver was designed. The output power of the LCC–LCC topology decreases with the decreasing coupling coefficient which offers a better controllability for the WPT system. To keep the receiver in resonance at the two charging distances, the coils should be carefully designed such that the inductance variation ratios of the main coil and the auxiliary coil due to the charging distance variation are the same. By setting the transmitters with different α_1 and different inverter DC voltages, the compatibility of 120 kW FWC and 7 kW NWC with the same receiver was achieved. Simulations were conducted to verify the design.

A downscaled prototype was built with a rated power level of 6.4 and 1.0 kW. The equal inductance variation ratios of the main coil and the auxiliary coil was achieved. The experimental results

Table 5 Simulations and measurements of the experimental prototype

System	Symbol	Turn Number	Simulation	Measurement	Error, %
FWC (0, 0)	L_{f1}	10	87.7 μH	86.0 μH	1.94
	L_1	15	281.8 μH	287.5 μH	−2.02
	L_{f21}	10	87.7 μH	85.9 μH	2.05
	L_{21}	15	281.8 μH	288.2 μH	−2.27
	k_{121}	-	0.783	0.780	0.38
NWC (0, 0)	L_{f3}	12	76.2 μH	74.6 μH	−2.10
	L_3	20	281.4 μH	281.9 μH	−0.18
	L_{f22}	10	61.0 μH	59.0 μH	3.28
	L_{22}	15	194.9 μH	195.4 μH	−0.26
	k_{232}	-	0.202	0.198	1.98
NWC (75 mm, 100 mm)	L_{f3}	12	76.1 μH	74.1 μH	2.70
	L_3	20	282.0 μH	282.9 μH	−0.32
	L_{f22}	10	60.9 μH	59.0 μH	3.22
	L_{22}	15	195.0 μH	196.3 μH	−0.66
	k_{232}	-	0.115	0.119	−3.36

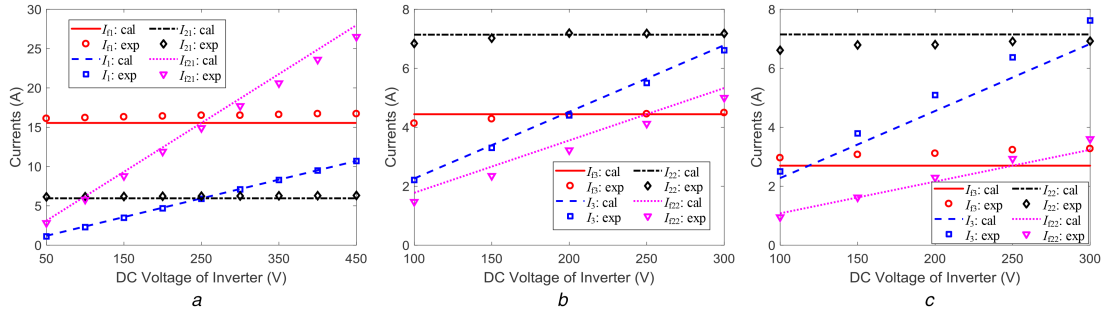

Fig. 13 *Calculated and measured current RMS values*
(a) 6.4 kW system at (0 mm, 0 mm),
(b) 1.0 kW system at (0 mm, 0 mm),
(c) 1.0 kW system at (75 mm, 100 mm)

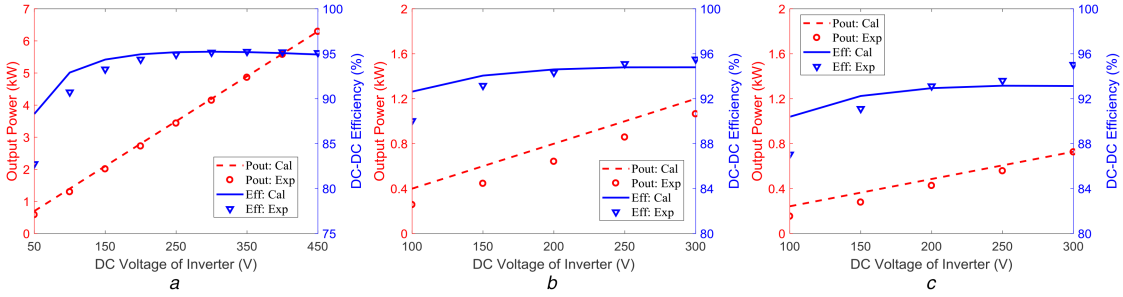

Fig. 14 *Calculated and measured output power and DC-DC efficiency*
(a) 6.4 kW system at (0 mm, 0 mm),
(b) 1.0 kW system at (0 mm, 0 mm),
(c) 1.0 kW system at (75 mm, 100 mm)

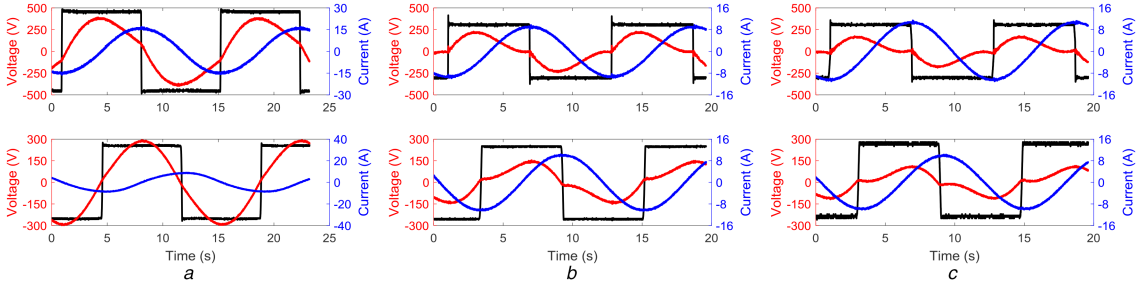

Fig. 15 *Experimental waveforms*
(a) 6.4 kW system at (0 mm, 0 mm),
(b) 1.0 kW system at (0 mm, 0 mm),
(c) 1.0 kW system at (75 mm, 100 mm)

showed that a DC–DC efficiency of over 95% can be achieved for the two different power levels with the same receiver.

6 Acknowledgments

The authors would like to thank Huawei Technologies CO., LTD for the support of this paper under grant no. 9406139, and the US Department of Energy for the support of this Study under the US-China Clean Energy Center – Clean Vehicle Consortium.

7 References

[1] Hui, S.Y.R.: 'Technical and safety challenges in emerging trends of near-field wireless power transfer industrial guidelines', *IEEE Electromagn. Compat. Mag.*, 2018, **7**, (1), pp. 78–86

[2] Zhang, Y., Zhao, Z., Lu, T.: 'Quantitative analysis of system efficiency and output power of four-coil resonant wireless power transfer', *IEEE J. Emerging Sel. Topics Power Electron.*, 2015, **3**, (1), pp. 184–190

[3] Huang, S., Li, Z., Lu, K.: 'Frequency splitting suppression method for four-coil wireless power transfer system', *IET Power Electron.*, 2016, **9**, (15), pp. 2859–2864

[4] Dai, X., Li, X., Li, Y., *et al.*: 'Impedance-matching range extension method for maximum power transfer tracking in IPT system', *IEEE Trans. Power Electron.*, 2018, **33**, (5), pp. 4419–4428

[5] Li, Y., Lin, T., Mai, R., *et al.*: 'Compact double-sided decoupled coils-based WPT systems for high-power applications: analysis, design, and experimental verification', *IEEE Trans. Transp. Electrification*, 2018, **4**, (1), pp. 64–75

[6] Guo, Y., Wang, L., Zhang, Y., *et al.*: 'Rectifier load analysis for electric vehicle wireless charging system', *IEEE Trans. Ind. Electron.*, 2018, **65**, (9), pp. 6970–6982

[7] Lee, E.S., Choi, J.S., Son, H.S., *et al.*: 'Six degrees of freedom wide-range ubiquitous IPT for IoT by DQ magnetic field', *IEEE Trans. Power Electron.*, 2016, **32**, (11), pp. 8258–8276

[8] Kan, T., Zhang, Y., Yan, Z., *et al.*: 'A rotation-resilient wireless charging system for lightweight autonomous underwater vehicles', *IEEE Trans. Veh. Technol.*, 2018, **67**, (8), pp. 6935–6942

[9] Yan, Z., Zhang, Y., Kan, T., *et al.*: 'Frequency optimization of a loosely coupled underwater wireless power transfer system considering eddy current loss', *IEEE Trans. Ind. Electron.*, 2019, **66**, (5), pp. 3468–3476

[10] Wikipedia.: 'Tesla supercharger', Available at: https://en.wikipedia.org/wiki/Tesla_Supercharger, 2018

[11] Baghdadi, M.E., Benomar, Y., Hegazy, O., *et al.*: 'Design approach and interoperability analysis of wireless power transfer systems for vehicular applications'. European Conf. on Power Electronics and Applications (EPE'16 ECCE Europe), Karlsruhe, Germany, 2016, pp. 1–11

[12] Zaheer, A., Hao, H., Covic, G.A., *et al.*: 'Investigation of multiple decoupled coil primary pad topologies in lumped ipt systems for interoperable electric vehicle charging', *IEEE Trans. Power Electron.*, 2015, **30**, (4), pp. 1937–1955

[13] Zhang, W., White, J.C., Abraham, A.M., *et al.*: 'Loosely coupled transformer structure and interoperability study for EV wireless charging systems', *IEEE Trans. Power Electron.*, 2015, **30**, (11), pp. 6356–6367

[14] Simon, O., Krempel, T., Wolf, H., *et al.*: 'Flexible secondary pad design for wireless power transfer providing public interoperability'. IEEE Int. Conf. on Environment and Electrical Engineering and 2017 IEEE Industrial and Commercial Power Systems Europe, Milan, Italy, 2017, pp. 1–7

[15] Lu, F., Zhang, H., Kan, T., *et al.*: 'A high efficiency and compact inductive power transfer system compatible with both 3.3 and 7.7 kW receivers'. IEEE Applied Power Electronics Conf. and Exposition (APEC), Tampa, FL,USA, 2017, pp. 3669–3673

[16] Zimmer, M., Heinrich, J., Parspour, N.: 'Design of a 3 kW primary power supply unit for inductive charging systems optimized for the compatibility to receiving units with 20 kW rated power'. Int. Electric Drives Production Conf. (EDPC), Nuremberg, Germany, 2014, pp. 1–5

[17] Hwang, J.T., Lee, D.S., Lee, J.H., *et al.*: 'An All-in-one (Qi, PMA and A4WP) 2.5 W fully integrated wireless battery charger IC for wearable applications'. IEEE Int. Solid-State Circuits Conf. (ISSCC), San Francisco, CA, USA, 2016, pp. 378–380

[18] Ahn, D., Kim, S., Kim, S., *et al.*: 'Wireless power transmitter and receiver supporting 200-kHz and 6.78-MHz dual-band operation without magnetic field canceling', *IEEE Trans. Power Electron.*, 2017, **32**, (9), pp. 7068–7082

[19] Li, S., Mi, C.: 'Wireless power transfer for electric vehicle applications', *IEEE J. Emerging Sel. Topics Power Electron.*, 2015, **3**, (1), pp. 4–17